Short-Range, Spin-Dependent Interactions of Electrons: A Probe for Exotic Pseudo-Goldstone Bosons

W. A. Terrano, E. G. Adelberger, J. G. Lee, and B. R. Heckel

Center for Experimental Nuclear Physics and Astrophysics, Box 354290, University of Washington,
Seattle, Washington 98195-4290, USA

We used a torsion pendulum and rotating attractor with 20-pole electron-spin distributions to probe dipole-dipole interactions mediated by exotic pseudo-Goldstone bosons with $m_b c^2 \leq 500 \ \mu$eV and coupling strengths up to 14 orders of magnitude weaker than electromagnetism. This corresponds to symmetry-breaking scales $F \leq 70$ TeV, the highest reached in any laboratory experiment. We used an attractor with a 20-pole unpolarized mass distribution to improve laboratory bounds on CP-violating monopole-dipole forces with $1.5 \ \mu$eV $< m_b c^2 < 400 \ \mu$eV by up to a factor of 1000.

Spontaneously broken global symmetries play an important role in particle physics [1]. When the underlying symmetry is exact, the process always produces massless pseudoscalar Goldstone bosons whose coupling to a fermion with mass m_f is $g_p = m_f/F$, where F is the energy scale of the spontaneously broken symmetry. If the symmetry is not exact but explicitly broken as well, as in the chiral symmetry of QCD, the fermionic couplings are unchanged, but the resulting pseudo-Goldstone bosons, such as the QCD pions, acquire a small mass $m_b = \Lambda^2/F$, where Λ is the explicit symmetry-breaking scale of the effective Lagrangian. Searches for the ultraweak, long-range interactions mediated by exotic pseudo-Goldstone bosons, therefore, provide very sensitive and general probes for new hidden symmetries broken at extremely high energies.

The tree-level potentials from pseudoscalar boson exchange are purely spin dependent. The classic pseudoscalar potential is the dipole-dipole interaction

$$V_{\text{dd}} = \frac{g_p^2 \hbar^2}{16\pi m_e^2 c^2 r^3} \left[(\hat{\boldsymbol{\sigma}}_1 \cdot \hat{\boldsymbol{\sigma}}_2)\left(1 + \frac{r}{\lambda}\right) \right.$$
$$\left. - 3(\hat{\boldsymbol{\sigma}}_1 \cdot \hat{\boldsymbol{r}})(\hat{\boldsymbol{\sigma}}_2 \cdot \hat{\boldsymbol{r}})\left(1 + \frac{r}{\lambda} + \frac{r^2}{3\lambda^2}\right) \right] e^{-r/\lambda}, \quad (1)$$

where $\lambda = \hbar/(m_b c)$. Axionlike bosons with an additional scalar coupling, g_S, can also generate a monopole-dipole interaction [2]

$$V_{\text{md}} = \frac{\hbar g_s g_p}{8\pi m_e c}\left[(\hat{\boldsymbol{\sigma}} \cdot \hat{\boldsymbol{r}})\left(\frac{1}{r\lambda} + \frac{1}{r^2}\right)\right] e^{-r/\lambda}. \quad (2)$$

Because these potentials average out to zero for unpolarized bodies, traditional searches for new macroscopic forces are essentially insensitive to such bosons. Motivated by theoretical conjectures that propose additional pseudo-Goldstone bosons such as axions, familons,

majorons, closed-string axions, and accidental pseudo-Goldstone bosons (see Ref. [3] for a recent review), we developed a generic "pseudo-Goldstone detector" with high sensitivity to both V_{dd} and V_{md} interactions. We combined the strategies of previous Eöt-Wash torsion-balance probes of electron-spin-dependent forces [4,5] (closed magnetic circuits containing high and low spin-density materials) and short-distance gravity [6,7] (m-fold azimuthally symmetric torsion-balance with rotating attractor devices that generate signal torques at m times the attractor frequency ω) to produce the instrument shown in Fig. 1.
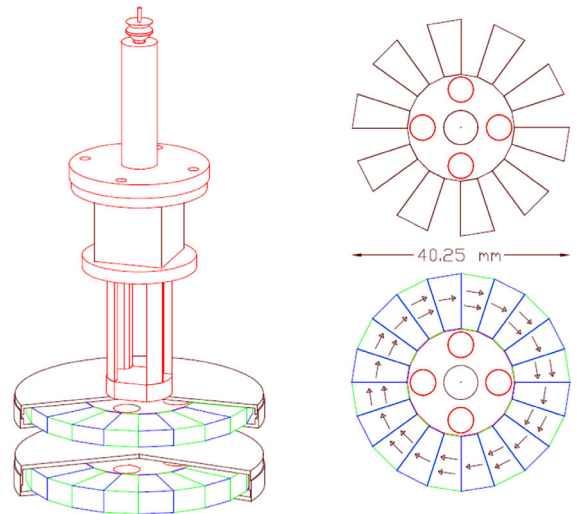
FIG. 1 (color online). (Left panel) The 20-pole spin pendulum and spin attractor; μ-metal cans on the pendulum and attractor are cut away to show the alnico (green) and SmCo$_5$ (blue) segments and one of the four pairs of calibration cylinders (red). The mirror cube was used to monitor the pendulum twist angle. The magnetic shield surrounding the entire pendulum is not shown. (Lower and upper right panels) Top views of the spin and mass attractors, respectively. Arrows indicate net spin density and direction.

The small scale of our device allowed us to probe V_{dd} interactions with $m_b c^2 \leq 500~\mu eV$, approximately 100 times heavier than previous studies with polarized electrons [5] and neutrons [8,9].

The key element of our instrument was a spin ring containing 20 equally magnetized segments of alternating high and low spin-density materials. This formed a spin 20 pole with a negligible external magnetic field. One spin ring was the active element of our detector, a torsion pendulum placed just above the rotating attractor. Our dipole-dipole search used an attractor consisting of a second 20-pole spin ring so that V_{dd} interactions would produce a 10ω torque on the pendulum as the attractor's high spin-density elements passed sequentially below the high or low spin-density segments of the pendulum. The sensitivity to V_{dd} or V_{md} interactions arises entirely from the spin-density contrast in the rings.

We used an unpolarized copper attractor that formed a mass 20 pole to measure the gravitational background in our V_{dd} study and to probe V_{md} interactions, both of which would produce 10ω torques. The pendulum and both attractors each contained four cylinders (tungsten and vacuum for the spin and mass attractors, respectively) that provided continuous 4ω gravitational calibration signals.

Alternating wedges of $SmCo_5$ and alnico provided the spin contrast of the rings. $SmCo_5$ has a substantial orbital contribution to its magnetic field [4], while alnico's magnetism comes almost entirely from polarized electrons. $SmCo_5$ fully magnetized to 9.8 kG contains $\sim 4.5 \times 10^{22}$ spins/cm^3, while alnico magnetized to the same degree has $\sim 8 \times 10^{22}$ spins/cm^3 [4]. The $SmCo_5$ wedges were cut from commercially magnetized material; the alnico was magnetized simply by assembling the ring. We tuned the precise magnetization of each alnico wedge *in situ* by applying a localized external field until the peak-to-peak leakage field 3 mm from the ring was reduced from ~ 100 to ~ 8 G. We then enclosed the ring assemblies in nested two-layer μ-metal cans with a total thickness of 0.53 mm, reducing the peak-to-peak residual field to $\sim 10~\mu G$. A 0.99 mm thick shielding screen consisting of 21 layers of alternating μ-metal and aluminum foils separated the attractor assembly from the pendulum. A 1.27 mm thick, cylindrical, μ-metal "house" surrounded the pendulum except for a hole for the suspension fiber and another that provided optical access to the pendulum; a 0.76 mm thick μ-metal tube surrounded the attractor turntable. The peak-to-peak magnetic field change at the pendulum location with the full shielding in place was below our resolution of $2~\mu G$.

Could the magnetic shielding also shield the V_{dd} and V_{md} interactions? We discuss this important point elsewhere [10] and show that, in our case, the effect is negligible. Briefly, if spins A and B are separated by a ferromagnetic shield (where the magnetization arises from electron spin), then V_{dd} and V_{md} are indeed shielded.

However, if spins A and B are surrounded by current coils that cancel their external magnetic fields, the shielding has little effect. In our case the $SmCo_5$'s orbital magnetic moment corresponds to the current coils.

The mass-density difference between $SmCo_5$ ($8.31~g/cm^3$) and alnico ($7.31~g/cm^3$) would produce a significant gravitational 10ω torque. We placed $76~\mu m$ thick W (Ti) shims above and below each alnico ($SmCo_5$) segment to minimize 10ω gravitational torques.

The active elements of the pendulum and attractor, along with the magnetic shielding, were installed in a rotating-attractor torsion balance normally used to study short-distance gravity. Details of that torsion balance and the general methods of data analysis are given in Refs. [6,7]. We centered and leveled the attractor ring to $\sim 15~\mu m$ of the turntable rotation axis with optical and mechanical techniques. We leveled the pendulum to $130~\mu m$ of its rotation axis using capacitive techniques, and we centered it to about $\pm 20~\mu m$ of the attractor rotation axis by maximizing the 4ω signal from the mass attractor. These misalignments were negligible relative to our typical separations $s \gtrsim 2$ mm. We inferred the vertical separation, s, between the bottom of the pendulum ring magnets and the top of the attractor magnets (or copper) using a z micrometer on the vertical translation stage that supported the suspension fiber. We measured the attractor-pendulum capacitance as a function of z and fitted these data to a finite-element electrostatic model to map the z-micrometer readings into the pendulum-screen separation. Mechanical and optical measurements provided the additional information needed to determine s.

The torque on the pendulum was inferred from a harmonic analysis of its twist angle, θ, as a function of the attractor angle $\phi = \omega t$. The data analysis procedure was similar to that used in Ref. [7]. The $\theta(\phi)$ time series was processed by a four-point digital filter that suppressed free torsional oscillations as well as the dc response and linear drift. Data runs were divided into cuts containing exactly one attractor revolution and each cut was fitted with a quadratic drift term plus the first 14 harmonics of the turntable angle. The harmonic amplitudes were corrected for pendulum inertia, electronic time constants, and the response of the digital filter. They were then converted into torques using the effective value of the fiber's torsional constant, $\kappa = I(2\pi/T_0)^2 = 3.1$ aN m/nrad, where T_0 is the pendulum's free oscillation period and its moment of inertia, $I = 134$ g cm^2, was computed from a detailed numerical model. T_0 was determined from "sweep runs" taken after each science run; the attractor turntable was stopped and the pendulum was given a $\sim 10~\mu rad$ kick. The resulting oscillations were analyzed to obtain a precise period and, crucially, to map out small nonlinearities in the autocollimator's analog position-sensitive detector. The measured 10ω and 4ω torques from a run were found by weighting equally all (typically 48) cuts in that run with
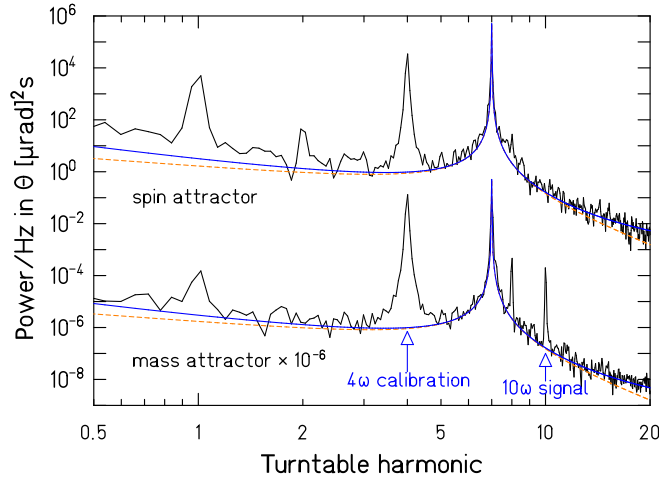
FIG. 2 (color online). Sample power spectral densities of the twist signals from the spin and mass attractors at the closest attained separations. The dashed lines show the thermal noise, and the solid lines include the effect of an additional $1/f^2$ component. The 8ω peak in the mass-attractor data is the first harmonic of the calibration signal. It is much smaller in the spin-attractor data because of its larger value of s.

the statistical uncertainties determined by the scatter of the results. These data were compared to those expected from the V_{dd} and V_{md} interactions and from gravity. The expected torques, assuming that the pendulum was aligned with the attractor, were computed using the Fourier-Bessel expansion, which converges rapidly for our application and requires only a single numerical integration [11].

The attractor rotation periods, $T_{att} = 7T_0$ or $6T_0$, were selected to place our 4ω and 10ω signals in low-noise regions (see Fig. 2). The noise was dominated by thermal fluctuations from internal losses in the suspension fiber, which gave the torsion oscillator a quality factor of $Q \approx 1500$.

Spin-attractor data were taken at $s = 4.12$, 5.13, and 8.15 mm (uncertainties are ± 0.015 mm). Because of the $1/r^3$ falloff of the potential, our V_{dd} sensitivity comes entirely from the $s = 4.12$ mm data. The results from 165 h of $s = 4.12$ mm data are shown in Table I. We expected the largest systematic effects with the spin attractor to be residual gravitational and magnetic couplings between the

TABLE I. Observed 4ω and 10ω torques. Amplitudes A are in units of aN m, phases ϕ are in degrees, and separations s are in millimeters. The 1σ uncertainties do not include systematic effects. If $V_{md} = 0$, we expect $\Delta\phi = \phi_{10\omega} - \phi_{4\omega} = -9.0°$.

Attractor	T_{att}/T_0	$A_{4\omega}$	$A_{10\omega}$	$\phi_{10\omega} - \phi_{4\omega}$
Spin: $s = 4.12$	7	2855 ± 5	0.7 ± 2.9	$+3 \pm 25$
Spin: $s = 4.12$	6	2863 ± 4	2.9 ± 2.8	-7.9 ± 5.5
Spin: $s = 4.12$	$6 + 7$	2860 ± 3	1.3 ± 2.0	-6.1 ± 8.6
Mass: $s = 1.98$	7	5611 ± 8	344 ± 4	-9.47 ± 0.08

pendulum and the attractor. Mass-attractor data supplemented by calculations showed that our shims reduced the gravitational component of $A_{10\omega}$ by 2 orders of magnitude to ~ 1 aN m. Measurements showed that the magnetic leakage field was fairly constant across all higher ($> 5\omega$) harmonics. We observed little evidence for such couplings (see Fig. 3), which would have produced torques at all of these frequencies as well as at 10ω. As a result, no corrections for magnetic backgrounds were necessary. Other systematic concerns such as thermal and electrostatic effects were found to be negligible. Our final value, including a gravitational systematic, is $A_{10\omega} = (1.3 \pm 2.2)$ aN m for a 95% confidence upper limit of $|A_{dd}| \leq 5.0$ aN m. The absolute value occurs because of the fourfold ambiguity in the attractor angle inferred from the 4ω signal. The corresponding constraints on a new dipole-dipole interaction, and the associated bounds on the symmetry-breaking scale F, are shown in Fig. 4. These are the most sensitive laboratory constraints on $(g_p^e)^2/\hbar c$ for $m_b \leq 500\ \mu eV/c^2$ (at the 5.5×10^{-17} level for $m_b < 30\ \mu eV/c^2$). To our knowledge, the only other laboratory constraints on pseudoscalars in this mass range are Ramsey's 1979 limit, $(g_p^p)^2/\hbar c < 3 \times 10^{-4}$ level [17], on anomalous spin-spin interactions between protons. Our results indicate that $F > 70$ TeV.

Because magnetic backgrounds in our V_{md} study using the mass attractor were small, we could use a single 0.25 mm thick μ-metal screen. This allowed us to take mass-attractor data at $s = 1.98$ mm as well as at 2.03, 3.00, 4.04, and 7.99 mm (uncertainties are $\pm .015$ mm). Our V_{md} constraints come entirely from the $s = 1.98$ mm data. The other data allowed us to check for systematics and validate our gravitational calculations. The observed 4ω and 10ω torques from 38 h of $s = 1.98$ mm data are shown in Table I. The gravitational contribution to the 10ω torque vanishes when the copper arms of the attractor are directly below the pendulum's $SmCo_5$ or alnico segments. This
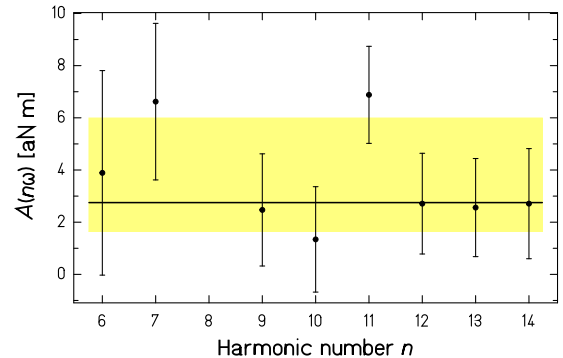
FIG. 3 (color online). Comparison of the spin-attractor 10ω science signal with nearby background signals. The shaded horizontal band indicates the mean and standard deviation, σ, of the background signals. The horizontal line shows the mean amplitude, $\sigma\sqrt{\pi/2}$, expected for random signals whose quadrature components have zero mean and spread σ.
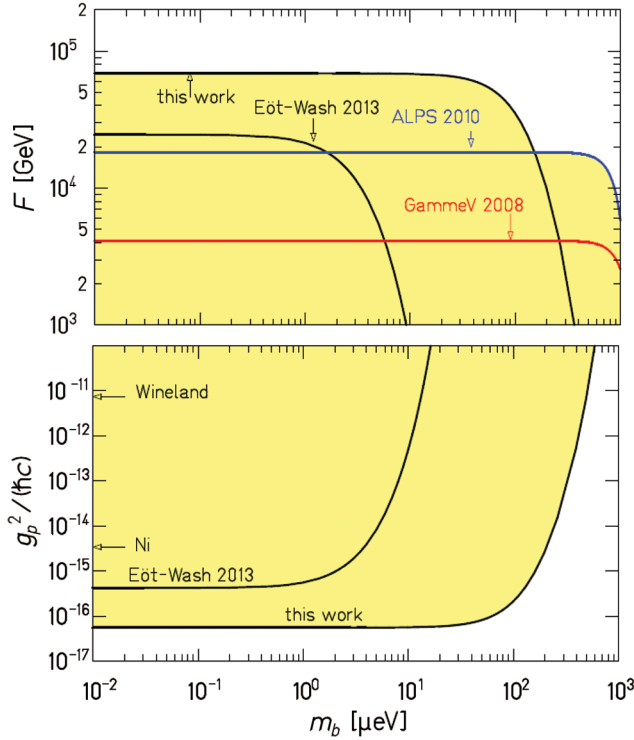
FIG. 4 (color online). (Bottom panel) Exotic dipole-dipole limits from this work and Ref. [5]. Arrows indicate the infinite-range constraints from Refs. [12,13]. Electron $g - 2$ constraints are at the 10^{-10} level [14]. (Top panel) Limits on the symmetry-breaking scale from this work and Refs. [15,16]. The shaded areas are excluded with 95% confidence.

FIG. 5 (color online). Monopole-dipole constraints from this work and Refs. [18–21]. The shaded region is excluded with 95% confidence. The $m_b = 0$ limit from Ref. [4] is 2×10^{-36}. (We doubled the 1σ limits given in Refs. [18,21]).

occurs (see Fig. 1) when the attractor is rotated 9° away from the angle at which calibration cylinders are aligned. Conversely, the V_{md} torque is maximal at those orientations. This allowed us to separate the effects of gravity from a V_{md} interaction. The V_{md} component of the 10ω torque is

$$|A_{\mathrm{md}}| = A_{10\omega}|\sin 10(\Delta\phi + \delta\phi)|, \qquad (3)$$

where $\Delta\phi = \phi_{10\omega} - \phi_{4\omega}$ and $\delta\phi$ is nominally 9°. Our A_{md} bound is dominated by the systematic uncertainty in $\delta\phi$. Alignment microscope measurements showed that the phase of the magnet ring relative to the calibration cylinders was only fixed to $\pm 0.17°$. An estimated 50 μm accuracy in positioning the gravitational shims, revealed by the behavior of $\phi_{10\omega}$ in our centering data, contributed an additional error of $\pm 0.29°$ and increased the uncertainty in $\delta\phi$ to $\pm 0.34°$. This gives a 1σ result $|A_{\mathrm{md}}| = (18 \pm 12)$ aN m with a 95% confidence upper limit, $|A_{\mathrm{md}}| \leq 38$ aN m. Our $|(g_p^e g_s^N)|/\hbar c$ constraint, shown in Fig. 5, improves upon previous work by up to a factor of 1000 for 1.5 μeV $\leq m_b c^2 \leq 400$ μeV. The most sensitive limit on $(g_p^n g_s^N)/\hbar c$ is also at the 10^{-28} level [22]. Stellar cooling rates [23] constrain V_{dd} interactions of simple pseudoscalar particles at a level well below our bound, and the astrophysics bound on g_p^e, combined with

bounds on g_s^N from the gravitational experiments, set very tight limits on V_{md} interactions between electrons and nucleons [24]. However, a chameleon mechanism could invalidate these astrophysical bounds while having a negligible effect in cooler, less dense lab environments [25]. In this case, V_{dd} and V_{md} can only be constrained by laboratory experiments such as this work, which reveals that any hidden symmetry involving electrons must be broken at an energy scale $F > 70$ TeV and, if it is explicitly broken as well, that scale Λ must be > 0.1 MeV. These set the highest laboratory bounds on the minimum energy scale of new hidden symmetries involving leptons. Extensions of general relativity that include torsion as well as curvature predict infinite-range dipole-dipole interactions [26] and are also constrained by this work.

[1] S. Weinberg, Phys. Rev. Lett. **29**, 1698 (1972).
[2] J. E. Moody and F. Wilczek, Phys. Rev. D **30**, 130 (1984).
[3] A. Ringwald, arXiv:1407.0546.
[4] B. R. Heckel, E. G. Adelberger, C. E. Cramer, T. S. Cook, S. Schlamminger, and U. Schmidt, Phys. Rev. D **78**, 092006 (2008).
[5] B. R. Heckel, W. A. Terrano, and E. G. Adelberger, Phys. Rev. Lett. **111**, 151802 (2013).
[6] C. D. Hoyle, D. J. Kapner, B. R. Heckel, E. G. Adelberger, J. H. Gundlach, U. Schmidt, and H. E. Swanson, Phys. Rev. D **70**, 042004 (2004).
[7] D. J. Kapner, E. G. Adelberger, J. H. Gundlach, B. R. Heckel, C. D. Hoyle, and H. E. Swanson, Phys. Rev. Lett. **98**, 021101 (2007).

[8] G. Vasilakis, J. M. Brown, T. W. Kornack, and M. V. Romalis, Phys. Rev. Lett. **103**, 261801 (2009).

[9] A. G. Glenday, C. E. Cramer, D. F. Phillips, and R. L. Walsworth, Phys. Rev. Lett. **101**, 261801 (2008).

[10] B. R. Heckel, E. G. Adelberger, and W. A. Terrano (to be published).

[11] W. A. Terrano, Ph.D. thesis, University of Washington, 2015.

[12] D. J. Wineland, J. J. Bollinger, D. J. Heinzen, W. M. Itano, and M. G. Raizen, Phys. Rev. Lett. **67**, 1735 (1991).

[13] W. T. Ni, T. C. P. Chui, S.-S. Pan, and B.-Y. Cheng, Physica (Amsterdam) **194B–196B**, 153 (1994).

[14] D. Hanneke, S. Fogwell, and G. Gabrielse, Phys. Rev. Lett. **100**, 120801 (2008).

[15] A. S. Chou, W. Wester, A. Baumbaugh, H. R. Gustafson, Y. Irizarry-Valle, P. O. Mazur, J. H. Steffen, R. Tomlin, X. Yang, and J. Yoo, Phys. Rev. Lett. **100**, 080402 (2008).

[16] K. Ehret *et al.*, Phys. Lett. B **689**, 149 (2010).

[17] N. F. Ramsey, Physica (Amsterdam) **96A**, 285 (1979).

[18] A. N. Youdin, D. Krause, K. Jagannathan, L. R. Hunter, and S. K. Lamoreaux, Phys. Rev. Lett. **77**, 2170 (1996).

[19] W. T. Ni, S.-S. Pan, H.-C. Yeh, L.-S. Hou, and J. Wan, Phys. Rev. Lett. **82**, 2439 (1999).

[20] G. D. Hammond, C. C. Speake, C. Trenkel, and A. P. Patón, Phys. Rev. Lett. **98**, 081101 (2007).

[21] S. A. Hoedl, F. Fleischer, E. G. Adelberger, and B. R. Heckel, Phys. Rev. Lett. **106**, 041801 (2011).

[22] K. Tullney, F. Allmendinger, M. Burghoff, W. Heil, S. Karpuk, W. Kilian, S. Knappe-Grüneberg, W. Müller, U. Schmidt, A. Schnabel, F. Seifert, Yu. Sobolev, and L. Trahms, Phys. Rev. Lett. **111**, 100801 (2013).

[23] G. Raffelt and A. Weiss, Phys. Rev. D **51**, 1495 (1995).

[24] G. Raffelt, Phys. Rev. D **86**, 015001 (2012).

[25] P. Jain and S. Mandal, Int. J. Mod. Phys. D **15**, 2095 (2006).

[26] W. T. Ni, Rep. Prog. Phys. **73**, 056901 (2010).